

Schrödinger's cat in an optical sideband

Takahiro Serikawa,¹ Jun-ichi Yoshikawa,^{1,2} Shuntaro Takeda,¹
Hidehiro Yonezawa,^{3,4} Timothy C. Ralph,^{4,5} Elanor H. Huntington,^{4,6}
Akira Furusawa^{1*}

¹Department of Applied Physics, School of Engineering,
The University of Tokyo, 7-3-1 Hongo, Bunkyo-ku, Tokyo, Japan.

²Quantum-Phase Electronics Center, School of Engineering,
The University of Tokyo, 7-3-1 Hongo, Bunkyo-ku, Tokyo, Japan.

³School of Engineering and Information Technology,
The University of New South Wales, Canberra, ACT 2600, Australia

⁴Center for Quantum Computation and Communication Technology,
Australian Research Council, Australia.

⁵School of Mathematics and Physics,
University of Queensland, Brisbane, QLD 4072, Australia.

⁶Research School of Engineering, College of Engineering and Computer Science,
Australian National University, Canberra, ACT 2600, Australia.

*To whom correspondence should be addressed; E-mail: akiraf@ap.t.u-tokyo.ac.jp.

Frequency multiplexing allows us to encode multiple quantum states on a single light beam. Successful multiplexing of Gaussian and non-Gaussian states potentially leads to scalable quantum computing or communication. Here we create an optical Schrödinger's cat state at a 500.6 MHz sideband, as a first step to non-Gaussian, frequency-division multiplexed photonic quantum information processing. The central idea is to use phase modulation as a frequency sideband beamsplitter in the photon subtraction scheme, where a small por-

tion of the sideband mode is downconverted to the carrier frequency to provide a trigger photon heralding the generation of a Schrödinger’s cat state. The reconstructed Wigner function of the cat state from a direct measurement of the 500 MHz sideband modes shows the negativity of $W(0,0) = -0.088 \pm 0.001$ without any corrections.

Multiplexing of optical modes has appeared as a promising technology for scalable photonic quantum information processing (QIP), where thousands of quantum states may be required for a practical computation or communication network. Time-division or frequency-division multiplexing provides the means of compact generations and manipulations of numerous quantum states. Recent demonstrations of large-scale continuous-variable (CV) cluster states (1) in time (2) and frequency (3) domains are such excellent examples. Employing the cluster states, CV one-way quantum computing model (4, 5) offers a framework of QIP, while ancillary non-Gaussian states are required for its universality (5–7). Therefore, implementation of non-Gaussian operations or creation of non-Gaussian states on multiplexed photonic modes is a key for universal and scalable photonic QIP. However, current technologies of frequency-division multiplexed quantum optics, including the cluster state generation, have been limited to Gaussian domain and lack the capability of performing universal quantum operations.

It has been desired and yet a challenging task to prepare non-Gaussian states on photonic modes that are suitable for multiplexing techniques. Photon subtraction (8) is a common method to create non-Gaussian states, and has been established on baseband photonic modes. An optical Schrödinger’s cat (SC) state is a famous example of such non-Gaussian states and can be created by means of subtracting a photon from a squeezed vacuum state (9–11). A SC state is a superposition of two macroscopic states, which is expressed in optics as $|\alpha\rangle + e^{i\psi} |-\alpha\rangle$, where $|\pm\alpha\rangle$ are coherent states of light with the opposite phases (8). SC states are powerful resources to implement several applications of QIP such as quantum error correction (12, 13) or

quantum computing based on coherent states (14). Besides, photon subtraction itself is a versatile technique (15) and has wide applications, such as quantum noiseless amplification (16), entanglement enhancement (17, 18), or a creation of particle-wave hybrid entanglement (19). Incorporating frequency-domain techniques in the photon subtraction scheme will lead to universal and practical quantum operations over multiplexed photonic modes, however it requires accessibility to an individual mode and careful considerations for resource states from which photons are subtracted.

Here we propose and demonstrate a method to create a SC state on a sideband photonic mode, in a manner that can be easily extended to creation of multiple non-Gaussian states on sideband modes of a single laser beam. The key idea is to employ a double sideband mode (DSB), i.e. a balanced superposition of upper and lower sideband modes around a carrier frequency, and implement photon subtraction on the DSB mode by coupling it with the baseband frequency mode. A DSB mode may correspond to amplitude or phase modulation, which is a natural basis for the frequency multiplexed QIP since it has a good compatibility with conventional quantum optical techniques. Multiple DSB modes are directly accessible by a single wideband homodyne measurement (20), and multiplexed displacement operation can be implemented by a single amplitude-phase modulator and a beamsplitter. In particular, highly-multiplexed, potentially over thousands, squeezed vacuum states in DSB modes are readily available by a continuously-pumped optical parametric oscillator (OPO) (3). Together with these basic CV QIP tools, photon subtraction on DSB modes complements a set of operations necessary to implement universal QIP on the sideband modes. Besides, DSB modes are free from technical noise of the carrier light, which enables shot-noise-limited measurement of the field amplitude, leading to, for example, an atomic quantum memory of a DSB light realized by measurement and feedback (21). Our method is compared with a pulse shaping of photon subtractors with frequency up-conversion suggested by Averchenko *et al.* (22) and recently

demonstrated by Ra *et al.* (23), in the sense that both access the coherent superposition of upper and lower frequency modes. In their method, however, higher order sideband modes have a complex pulse shape so as to achieve orthogonality in the pulsed regime. Our techniques developed here can move to higher order sidebands while keeping the shape of the envelope and thus opens up a new regime of the frequency-multiplexed photonic QIP in a scalable manner.

Figure 1 (a) shows a schematic of our setup. A SC state is created by subtracting a photon from a DSB mode of a squeezed vacuum state, which is prepared by an OPO. A frequency sideband beamsplitter, which transfers an optical component at a given frequency to both upper and lower sidebands, is realized with a small phase modulation (24). In the Heisenberg picture, weak frequency- Ω modulation transforms \hat{a}_ω , an annihilation operator for a mode at frequency ω , as

$$\hat{a}_\omega^{\text{mod}} \sim \sqrt{1 - \frac{\beta^2}{2}} \hat{a}_\omega + \frac{\beta}{2} (e^{i\theta} \hat{a}_{\omega+\Omega} + e^{-i\theta} \hat{a}_{\omega-\Omega}), \quad (1)$$

where $\beta \ll 1$ expresses the modulation depth and θ is determined by the modulation phase. We set the modulation frequency Ω to a resonant frequency of the OPO so that photons at upper and lower sidebands $\omega_0 \pm \Omega$ are transferred to the carrier ω_0 . Subsequent photon detection at the carrier frequency leads to a superposition of states with a photon being subtracted from upper and lower sidebands, thus heralds a SC state creation on the DSB mode. This method creates a superposition of upper and lower sideband states with the simple setup, which is challenging if we use a straightforward implementation of frequency-domain interaction, i.e. frequency separation, shift and mixing.

A DSB mode is described as $(e^{i\theta} \hat{a}_\Omega + e^{-i\theta} \hat{a}_{-\Omega})/\sqrt{2}$, which has a real, sinusoidal envelope with a phase θ in time-domain. Note that hereafter we omit the carrier frequency ω_0 unless otherwise noted. Here, corresponding to two degrees of freedom of \hat{a}_Ω and $\hat{a}_{-\Omega}$, DSB modes at frequency Ω are decomposed into two quadrature phase components, namely *cos-sideband* $\hat{a}_\Omega^{\text{cos}} = (\hat{a}_\Omega + \hat{a}_{-\Omega})/\sqrt{2}$ and *sin-sideband* $\hat{a}_\Omega^{\text{sin}} = (\hat{a}_\Omega - \hat{a}_{-\Omega})/\sqrt{2}i$. While dealing with high-

frequency DSB modes often presents a challenge to selectively access one of them, a strong advantage of our method is that we can select the cos-sideband, or any superposition of two DSB modes, since θ is controllable by tuning the modulation phase.

The output of a continuously-pumped OPO can be factorized in the sin- and cos-sideband modes (25). Independent squeezed states are prepared on both DSB modes at the resonant frequencies. Our OPO is resonant at ± 500.6 MHz and the carrier frequency mode is kept vacuum (Fig. 1B), where we carefully identify the free spectral range of the OPO at $2\Omega = 1001.2$ MHz to determine the sideband frequency. To describe our scheme, we focus on the DSB modes at the resonance Ω and the carrier mode. The output of the OPO is expressed as

$$|\Psi_0\rangle = |0\rangle_{\text{carrier}} \otimes |\text{SQ}\rangle_{\text{cos}} \otimes |\text{SQ}\rangle_{\text{sin}}, \quad (2)$$

where $|0\rangle_{\text{carrier}}$ is a vacuum state of the carrier mode \hat{a}_0 and $|\text{SQ}\rangle_{\text{cos,sin}}$ are squeezed states of $\hat{a}_\Omega^{\text{cos}}$ and $\hat{a}_\Omega^{\text{sin}}$, respectively. Note that the effect of the finite linewidth of the OPO, which corresponds to the finite correlation time of the squeezed state, is ignored here; for further analysis, see (26).

Photon subtraction is completed by modulating the squeezed light and detecting the carrier frequency photon with an avalanche photodiode (APD) and a frequency separator. In order to apply phase modulation without inducing decoherence, we use a homemade bulk electro-optic modulator (EOM) that has low-optical loss below 0.5%. By adjusting the phase of the driving signal of the EOM, cos-sideband mode is selectively downconverted to the carrier, i.e. θ in Eq. (1) is set at zero. The frequency separator, consisting of three optical cavities in the real experiment, extracts the carrier frequency component and guide it to the trigger mode. Trigger clicks of the APD herald photon subtraction events, which can be expressed as conditioning by a single-photon state of the trigger mode as

$$\text{trigger}\langle 1| = \text{carrier}\langle 0| \left[\hat{a}_0 + \frac{\beta}{\sqrt{2}} \hat{a}_\Omega^{\text{cos}} \right], \quad (3)$$

where the creation operator of the trigger mode is reduced to the signal modes by Eq.(1), and

the transfer efficiency β^2 is set at 0.020. Conditioned by Eq.(3), Eq.(2) yields a minus SC state in the cos-sideband mode, while the sin-sideband mode remains as a squeezed vacuum state:

$$|\Psi_{\text{cat}}\rangle \propto_{\text{trigger}} \langle 1 | \Psi_0 \rangle \propto \hat{a}_{\Omega}^{\text{cos}} |\text{SQ}\rangle_{\text{cos}} \otimes |\text{SQ}\rangle_{\text{sin}}. \quad (4)$$

Note that the SC state actually has a wavepacket-like mode around the trigger time τ with an envelope of $\cos \Omega t \xi(t - \tau)$, due to the frequency correlation of the squeezed state and the frequency separator.

The quadrature distributions of the sin- and cos-sideband modes are measured by homodyne detection with an optical local oscillator (LO) at the carrier frequency, where 83% of effective detection efficiency is realized at $\Omega = 500.6$ MHz by a low-loss, low-noise resonant homodyne detector (27). The two DSBs are electrically resolved by an IQ demodulator with an pre-defined electrical LO proportional to $\cos \Omega t$. Driven by the trigger signals, the in-phase (cos-sideband) and quadrature (sin-sideband) signals are simultaneously digitized and 8,000 samples of quadrature signals for each 36 equally partitioned optical phases are collected.

The envelope function $\xi(t)$ of the SC states are identified by independent component analysis (28) of the demodulated cos-sideband waveforms and shown in Fig. 2A. The quadrature of the wavepacket of SC states is obtained by integrating the demodulated in-phase homodyne signal weighted by $\xi(t)$. In order to discuss the sideband-selectivity of our method, we also extract the quadrature of the sin-sideband wavepacket that has the same envelope as the subtracted state (Fig. 2B). Note that the duration of the envelope is determined by the OPO's correlation time and the time constant of the separator, which are tunable parameters, and it can be matched to external devices such as optical memories (26).

The quadrature distributions of cos- and sin-sideband wavepacket modes clearly show the effect of subtraction (Fig. 3A), where only the cos-sideband state is reshaped by the coincidences of the triggers. In the cos-sideband mode, two sinusoidal-wave-like traces are over-

lapped, indicating the superposed coherent states $|\pm\alpha\rangle$ with the interference fringe at the intersection as an evidence of the coherence.

The non-Gaussian nature of the generated SC state is confirmed by the negativity of the Wigner function obtained by maximum-likelihood estimation (29) (Fig. 3B). The cos-sideband state shows $W_{\text{cos}}(0,0) = -0.088 \pm 0.001$ ($\hbar = 1$) without loss correction, which is to be compared with the negative peak of the pure SC states $W_{\text{cat}}(0,0) = -1/\pi$. The fidelity of the cos-sideband state to the best-fit minus cat state $|\Psi\rangle = \mathcal{N}[|\alpha\rangle - |-\alpha\rangle]$, with the coherent state amplitude $\alpha = 0.88 - 0.19i$, is 64%. Both optical losses and contamination from the sin-sideband contribute to $W(0,0)$ as a mixture of plus value $1/\pi$. In this sense, when the measured total efficiency $\eta^{\text{cos}} = 0.68$ is considered, we expect $W_{\text{cos}}(0,0) = -0.114$. To fit the actual value of $W_{\text{cat}}(0,0)$, 4% of mixture of background squeezed state is presumed where the fake clicks of the APD and the impurity from the inherent mode-mismatch of photon subtraction (30) contributes 0.8% and 3.0% to it respectively. Thus the upper bound of the mixture of the sin-sideband component is estimated below 1%. The sin-sideband mode has 99.9% fidelity to the lossy squeezed state since it is untouched by the subtraction. There is no intrinsic limit to the purity of the photon subtraction process that can be obtained by our method; the current imperfections come from technical limitations (26).

In conclusion, we have realized a highly pure photon subtractor that operates on high-frequency sideband modes of light. Our scheme can be extended to the creation of further SC states on higher frequency sidebands by adding sets of a modulator, a separator and an APD. It is notable that two quadrature sideband modes at one frequency are also useful for dual-rail encoding of quantum states. Since the DSB encoding (cos- and sin-sideband modes) and single-sideband encoding (upper and lower sideband modes) are connected by effective beamsplitter transformations, these encoding can be used for a single-beam implementations of quantum teleportation (31) or cat breeding protocols (32).

References

1. J. Zhang, S. L. Braunstein, *Phys. Rev. A* **73**, 032318 (2006).
2. S. Yokoyama, *et al.*, *Nature Photonics* **7**, 982 (2013).
3. M. Chen, N. C. Menicucci, O. Pfister, *Phys. Rev. Lett.* **112**, 120505 (2014).
4. R. Raussendorf, H. J. Briegel, *Phys. Rev. Letters* **86**, 5188 (2001).
5. N. C. Menicucci, *et al.*, *Phys. Rev. Lett.* **97**, 110501 (2006).
6. S. Lloyd, S. L. Braunstein, *Phys. Rev. Lett.* **82**, 1784 (1999).
7. R. Filip, P. Marek, U. L. Andersen, *Phys. Rev. A* **71**, 042308 (2005).
8. M. Dakna, T. Anhut, T. Opatrný, L. Knöll, D.-G. Welsch, *Phys. Rev. A* **55**, 3184 (1997).
9. A. Ourjoumtsev, R. Tualle-Brouri, J. Laurat, P. Grangier, *Science* **312**, 83 (2006).
10. J. S. Neergaard-Nielsen, B. M. Nielsen, C. Hettich, K. Mølmer, E. S. Polzik, *Phys. Rev. Lett.* **97**, 083604 (2006).
11. A. Ourjoumtsev, H. Jeong, R. Tualle-Brouri, P. Grangier, *Nature* **448**, 784 (2007).
12. Z. Leghtas, *et al.*, *Phys. Rev. Lett.* **111**, 120501 (2013).
13. N. Ofek, *et al.*, *Nature* **536**, 441 (2016).
14. T. C. Ralph, A. Gilchrist, G. J. Milburn, W. J. Munro, S. Glancy, *Phys. Rev. A* **68**, 042319 (2003).
15. M. S. Kim, *J. Phys. B* **41**, 133001 (2008).
16. A. Zavatta, J. Fiurášek, M. Bellini, *Nature Photonics* **5**, 52 (2011).

17. C. Navarrete-Benlloch, R. García-Patrón, J. H. Shapiro, N. J. Cerf, *Phys. Rev. A* **86**, 012328 (2012).
18. T. J. Bartley, *et al.*, *Phys. Rev. A* **87**, 022313 (2013).
19. O. Morin, *et al.*, *Nature Photonics* **8**, 570 (2014).
20. T. C. Ralph, E. H. Huntington, T. Symul, *Phys. Rev. A* **77**, 063817 (2008).
21. B. Julsgaard, J. Sherson, J. I. Cirac, J. Fiurášek, E. S. Polzik, *Nature* **432**, 482 (2004).
22. V. A. Averchenko, V. Thiel, N. Treps, *Phys. Rev. A* **89**, 063808 (2014).
23. Y.-S. Ra, C. Jacquard, A. Dufour, C. Fabre, N. Treps, *Phys. Rev. X* **7**, 031012 (2017).
24. J. Capmany, C. R. Fernández-Pousa, *J. Opt. Soc. Am. B* **27**, A119 (2010).
25. A. E. Dunlop, E. H. Huntington, C. C. Harb, T. C. Ralph, *Phys. Rev. A* **73**, 013817 (2006).
26. Materials and methods are available as supplementary materials on Science Online.
27. T. Serikawa, A. Furusawa, <https://arxiv.org/abs/1803.06462> (2018).
28. P. Comon, *Signal processing* **36**, 287 (1994).
29. A. Lvovsky, *J. Opt. B: Quantum Semiclass. Opt.* **6**, S556 (2004).
30. J. Yoshikawa, W. Asavanant, A. Furusawa, *Phys. Rev. A* **96**, 052304 (2017).
31. H. Song, H. Yonezawa, K. B. Kuntz, M. Heurs, E. H. Huntington, *Phys. Rev. A* **90**, 042337 (2014).
32. D. V. Sychev, *et al.*, *Nature Photonics* **11**, 379 (2017).
33. J. Appel, D. Hoffman, E. Figueroa, A. I. Lvovsky, *Phys. Rev. A* **75**, 035802 (2007).

34. B. Efron, R. Tibshirani, *Statistical science* pp. 54–75 (1986).

Acknowledgments

Funding: This work was supported by CREST (JPMJCR15N5) of JST, JSPS KAKENHI, and the Australian Research Council Centre of Excellence for Quantum Computation and Communication Technology (Project No. CE170100012). **Author contributions:** Conceptualization, T.C.R., E.H.H., H.Y. and A.F.; Methodology, T.S. and J.Y.; Investigation, T.S.; Writing , T.S., J.Y., S.T., H.Y., T.C.R., E.H.H. and A.F.; Supervision, T.C.R., E.H.H., H.Y. and A.F. **Competing interests:** None declared. **Data and materials availability:** All data supporting our result is available in the manuscript or the supplementary materials.

Supplementary materials

Supplementary Text

Materials and Methods

Figs. S1 to S7

Table S1

References (33–34)

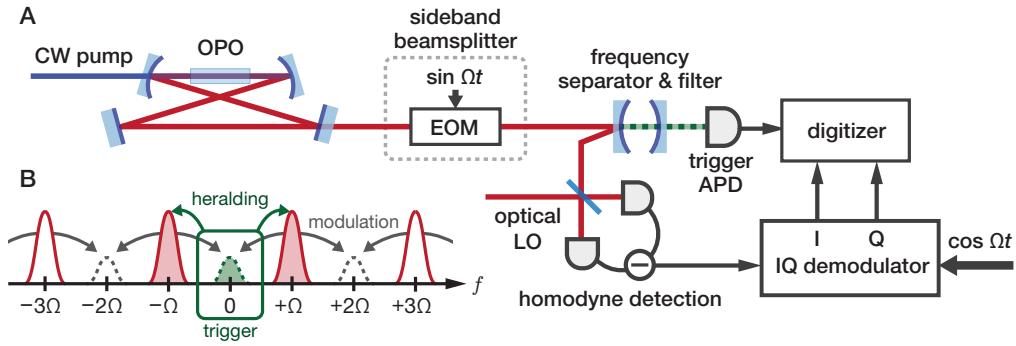


Fig. 1. (A) Schematic of the experiment and (B) frequency structure of the OPO resonance (red line), phase modulation (gray arrow), and trigger line filter (green box). OPO: optical parametric oscillator; CW: continuous-wave; APD: avalanche photodiode; EOM: electro-optic modulator; LO: local oscillator. I and Q denote in-phase and quadrature signal.

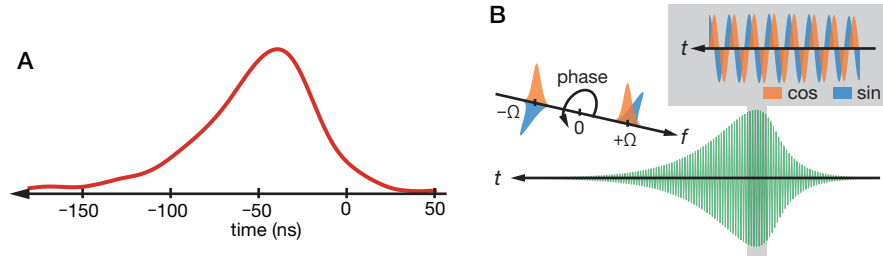


Fig. 2. (A) Estimated envelope function $\xi(t)$ of the sideband wavepacket of the subtracted mode. The time origin is placed at the trigger time. (B) Conceptual sketch of cos- and sin-sideband wavepackets.

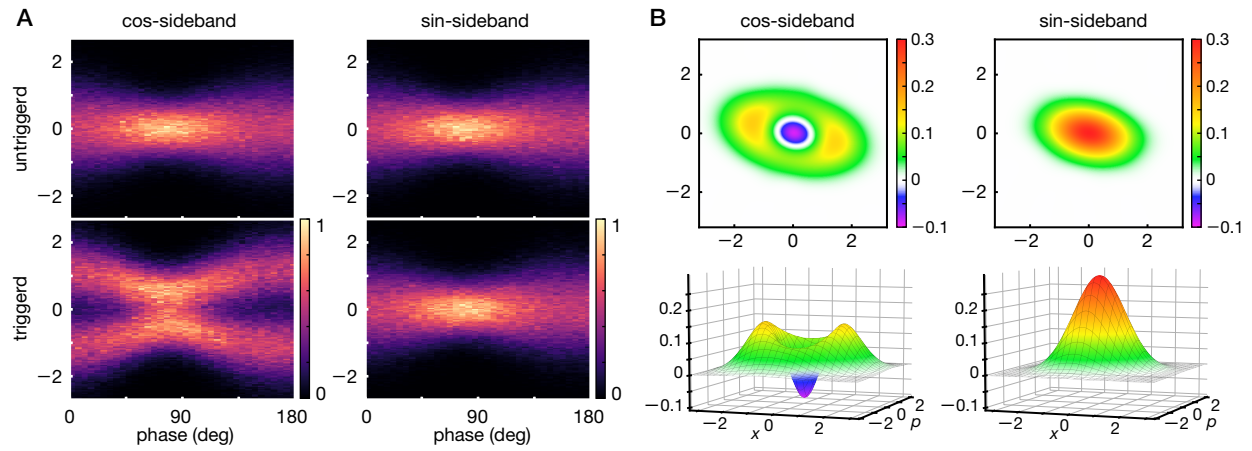


Fig. 3. (A) Quadrature distributions of 36 phase slices ($\hbar = 1$). Upper row: recorded regardless of trigger. Lower row: triggered. (B) Reconstructed Wigner functions. This is directly observed data and no analytical corrections for experimental imperfections are applied.

Supplementary Materials for Schrödinger's cat in an optical sideband

Takahiro Serikawa, Jun-ichi Yoshikawa, Shuntaro Takeda, Hidehiro Yonezawa,
Timothy C. Ralph, Elanor H. Huntington, Akira Furusawa*

*To whom correspondence should be addressed; E-mail: akiraf@ap.t.u-tokyo.ac.jp.

This PDF file includes:

Supplementary Text
Materials and Methods
Figs. S1 to S7
Table S1

Supplementary Text

Model of sideband squeezing

The linewidth of an optical parametric oscillator (OPO) induces finite time correlation of the output squeezed state. In this section, we describe the broadband squeezing operation induced by an OPO to deduce the squeezing spectrum and time correlation of sideband squeezed states. The unit of $\hbar = 1$ is adopted throughout this supplementary material. A degenerate OPO pumped by a frequency $2\omega_0$ beam generates entangled photon pairs at frequency $\omega_0 + \omega$ and $\omega_0 - \omega$, which leads to a two-mode squeezed vacuum state in the frequency-domain expressed as,

$$|\psi\rangle_{\text{OPO}} = \exp \left[\int_0^\infty d\omega \left(r^*(\omega) \hat{a}_\omega^\dagger \hat{a}_{-\omega}^\dagger - r(\omega) \hat{a}_\omega \hat{a}_{-\omega} \right) \right] |0\rangle \quad (5)$$

where $|0\rangle$ is the vacuum state vector, \hat{a}_ω is the annihilation operator of the frequency ω light on a rotating frame at ω_0 , and $r(\omega)$ denotes the correlation function of the OPO. We introduce double sideband (DSB) modes $\hat{\tilde{a}}_\omega^\theta = [e^{i\theta} \hat{a}_\omega + e^{-i\theta} \hat{a}_{-\omega}] / \sqrt{2}$, where we define θ as the sideband phase and tilde indicates that it is a sideband operator. Corresponding to the two degrees of freedom of $+\omega$ and $-\omega$ modes, the DSB modes in frequency ω are decomposed into two orthogonal modes, which can be represented by $\hat{\tilde{a}}_\omega^{\cos}$ and $\hat{\tilde{a}}_\omega^{\sin}$ where θ is 0 and $\pi/2$, respectively. With this basis, the OPO is reinterpreted as two photon creation / annihilation process, yielding two separable squeezed vacua as $|\psi\rangle_{\text{OPO}} = \hat{\tilde{S}}_r^{\cos} |0\rangle_{\cos} \otimes \hat{\tilde{S}}_r^{\sin} |0\rangle_{\sin}$, where $\hat{\tilde{S}}_r^j$ is the multi-mode

squeezing operator characterized by the frequency-dependent squeezing level $r(\omega)$,

$$\hat{S}_r^i = \exp \left[\frac{1}{2} \int_0^\infty d\omega \left(r^*(\omega) (\hat{a}_\omega^{i\dagger})^2 - r(\omega) (\hat{a}_\omega^i)^2 \right) \right], \quad (6)$$

where $i = \cos, \sin$ specifies one of the DSB basis. This is equivalent to the Bogoliubov transformations in each sideband mode expressed in the Heisenberg picture as

$$\hat{S}_r^{i\dagger} \hat{a}_\omega \hat{S}_r^i = \cosh |r(\omega)| \hat{a}_\omega^i + e^{i \text{Arg} r(\omega)} \sinh |r(\omega)| \hat{a}_\omega^{i\dagger}. \quad (7)$$

The quadrature operator of a sideband mode along the phase ϕ is defined as

$$\hat{x}_\omega^i(\phi) = \frac{1}{2} \left(e^{i\phi} \hat{a}_\omega^i + e^{-i\phi} \hat{a}_\omega^{i\dagger} \right). \quad (8)$$

Equation (7) gives quadrature squeezing

$$\hat{S}_r^{i\dagger} \hat{x}_\omega^i(\phi) \hat{S}_r^i = \left| \cosh |r(\omega)| + e^{-i(2\phi + \text{Arg} r(\omega))} \sinh |r(\omega)| \right| \hat{x}_\omega^i(\phi'). \quad (9)$$

Here,

$$\phi' = \text{Arg} \left[e^{-i\phi} \cosh |r(\omega)| + e^{-i(\phi + \text{Arg} r(\omega))} \sinh |r(\omega)| \right] \quad (10)$$

expresses the phase shift effect, which can be ignored when we consider vacuum squeezing $\hat{S}_r^i |0\rangle$, since the quadrature operator is phase-insensitive for the initial vacuum state. Anti-squeezing / squeezing is realized at $2\phi + \text{Arg} r(\omega) = 0, \pi/2$ respectively and then the quadrature variances $\tilde{V}(\omega; \phi) = \langle \hat{x}_\omega^i(\phi)^2 \rangle$ read

$$\tilde{V}(\omega; -\text{Arg} r(\omega)/2) = \frac{1}{2} e^{2|r(\omega)|}, \quad (11)$$

$$\tilde{V}(\omega; \pi/4 - \text{Arg} r(\omega)/2) = \frac{1}{2} e^{-2|r(\omega)|}. \quad (12)$$

The general form of the squeezing level spectrum $r(\omega)$ is given in reference (25). When we assume the frequency structure of the OPO to be symmetric about ω_0 and the pump phase to be zero, $r(\omega)$ is real regardless of ω , giving

$$r(\omega) = \ln \left| \frac{(\gamma + \varepsilon)^2 - \left(\frac{1 \pm e^{i\omega\delta}}{\delta} \right)^2}{\left(\gamma - \frac{1 \pm e^{i\omega\delta}}{\delta} \right)^2 - \varepsilon^2} \right|, \quad (13)$$

where γ is the cavity decay constant, ε is the pump parameter, and δ is the round-trip time of the cavity. Periodic structure appears in $e^{i\omega\delta}$ suggesting $2\pi/\delta$ as the free spectral range (FSR)

of the OPO, which we define as 2Ω . In this formula, \pm corresponds to the two possibility of the OPO resonance condition, i.e, $-$ for when the OPO is resonant at $\omega = 0$ and $+$ for when the OPO is anti-resonant. Here, we consider the latter case and focus on the lowest-frequency resonance. The squeezing spectrum is approximated around $\omega = \Omega$, leading to

$$r(\omega) \approx \ln \left| \frac{\gamma + \varepsilon + i(\omega - \Omega)}{\gamma - \varepsilon - i(\omega - \Omega)} \right|. \quad (14)$$

This form is justified when each resonant peak of the OPO is narrow and well separated from each other, as is the case in our experiment. When the pump field is weak, Eq. (14) is further approximated,

$$r(\omega) \approx \frac{2\gamma\varepsilon}{\gamma^2 + (\omega - \Omega)^2}, \quad (15)$$

giving a Lorentzian spectrum around the resonance at Ω .

These frequency-domain analyses are exported to a time-domain description by introducing instantaneous mode operators

$$\hat{a}_t = \frac{1}{\sqrt{2\pi}} \int d\omega e^{i\omega t} \hat{a}_\omega. \quad (16)$$

Sideband modes are sine and cosine transforms of \hat{a}_t ;

$$\hat{a}_\omega^{\cos} = \frac{1}{\sqrt{2\pi}} \int dt \cos \omega t \hat{a}_t, \hat{a}_\omega^{\sin} = \frac{1}{\sqrt{2\pi}} \int dt \sin \omega t \hat{a}_t. \quad (17)$$

The inverse transformation of Eq. (17) is

$$\hat{a}_t = \frac{1}{\sqrt{2\pi}} \int d\omega \left(\cos \omega t \hat{a}_\omega^{\cos} + \sin \omega t \hat{a}_\omega^{\sin} \right). \quad (18)$$

Equation (5) is transformed as

$$|\psi\rangle_{\text{OPO}} = \exp \left[\int dt_1 dt_2 \left(R^*(t_1 - t_2) \hat{a}_{t_1}^\dagger \hat{a}_{t_2}^\dagger - R(t_2 - t_1) \hat{a}_{t_1} \hat{a}_{t_2} \right) \right] |0\rangle, \quad (19)$$

where the time-domain correlation function $R(t)$ is defined by

$$R(t) = \frac{1}{\sqrt{2\pi}} \int d\omega e^{-i\omega t} r(\omega). \quad (20)$$

When we place the assumptions above, $R(t)$ is derived from Eq. (15) as

$$R(t) = \sqrt{2\pi}\varepsilon \exp(-\gamma|t| - i\Omega t). \quad (21)$$

Defining the double-sided decay function of the OPO as $h(t) = \exp(-\gamma|t|)$, the time correlation of the first sideband squeezing is considered to be a product of cavity decay $h(t)$ and sideband-frequency rotation $\exp(-i\Omega t)$.

Model of sideband photon subtraction

In this section, we describe photon subtraction from a DSB mode and analyze the effect on the sideband squeezed state. We show that optical Schrödinger's cat (SC) states are generated on wavepackets, whose envelope is determined by the response of frequency filters and the OPO's time correlation.

To clarify the merit of the proposed method, we first consider a simpler way of photon subtraction from sideband, where a frequency filter picks up the upper and lower band component of a sideband squeezed state and a photon detection at these bands heralds a subtraction event. This is a *passive* process and does not discriminate cos- and sin-sidebands, as a result of the time translation symmetry of the setup. Our scheme, in contrast, uses an *active* process, where the phase-modulation selects one fixed DSB mode synchronized with an external reference frame.

Figure S1A shows a rough sketch of passive subtraction from a DSB mode. A small portion ζ of the light is picked up to the trigger mode \hat{a}_t^{trig} by a beamsplitter operation \hat{B} :

$$\hat{B}^\dagger \hat{a}_t^{\text{trig}} \hat{B} = \sqrt{1-\zeta} \hat{a}_t^{\text{trig}} + \sqrt{\zeta} \hat{a}_t. \quad (22)$$

The frequency filter \mathcal{F} is placed to extract the first sideband component around $\pm\Omega$. We adopt Eq. (15) for the expression of the sideband squeezing, where the higher order resonances of the OPO are ignored since they are filtered out. Subsequently an avalanche photo diode (APD) detects a photon at $t = \tau$, providing the conditioned state

$$|\psi\rangle_\tau = \mathcal{N} \left[\text{trig} \langle 0 | \hat{a}_\tau^{\text{trig}} \hat{B} | \psi \rangle_{\text{OPO}} | 0 \rangle_{\text{trig}} \right], \quad (23)$$

where \mathcal{N} is renormalization. Considering Eq.(22), this results in

$$|\psi\rangle_\tau = \mathcal{N} \left[\text{trig} \langle 0 | \hat{B} \left(\hat{a}_\tau | \psi \rangle_{\text{OPO}} \right) | 0 \rangle_{\text{trig}} \right]. \quad (24)$$

Thus the conditioned state is a photon subtracted state with an optical loss of ζ induced by \hat{B} . Using Eqs. (6) and (18),

$$\hat{a}_\tau | \psi \rangle_{\text{OPO}} \propto \int d\omega \left(\cos \omega \tau \hat{a}_\omega^{\text{cos}} + \sin \omega \tau \hat{a}_\omega^{\text{sin}} \right) \left(\hat{\mathcal{S}}_r^{\text{cos}} | 0 \rangle_{\text{cos}} \otimes \hat{\mathcal{S}}_r^{\text{sin}} | 0 \rangle_{\text{sin}} \right). \quad (25)$$

Here we set $\tau = 0$, in other words, the origin of sideband phase is re-defined by the photon detection timing. Then the photon is subtracted from cos-sideband and the two-mode states are factorized in the DSB basis.

$$\hat{a}_0 | \psi \rangle_{\text{OPO}} \propto \left(\int d\omega \hat{a}_\omega^{\text{cos}} \hat{\mathcal{S}}_r^{\text{cos}} | 0 \rangle_{\text{cos}} \right) \otimes \left(\hat{\mathcal{S}}_r^{\text{sin}} | 0 \rangle_{\text{sin}} \right). \quad (26)$$

Now we show that the photon-subtracted cos-sideband mode is in a squeezed single photon state, i.e. an SC state (8). Equation (7) and (14) lead to

$$\int d\omega \hat{a}_\omega^{\text{cos}} \hat{S}_r^{\text{cos}} |0\rangle_{\text{cos}} = \hat{S}_r^{\text{cos}} \int d\omega \sinh r(\omega) \hat{a}_\omega^{\dagger \text{cos}} |0\rangle_{\text{cos}}, \quad (27)$$

where $\int d\omega \sinh r(\omega) \hat{a}_\omega^{\dagger \text{cos}} |0\rangle_{\text{cos}}$ expresses a single photon state in cos-sideband wavepacket. In the weak pumping regime, $\sinh r(\omega)$ is near to $r(\omega)$ and we can assume Eq. (15), resulting in the time-domain expression of the single photon state wavepacket:

$$\int d\omega \sinh r(\omega) \hat{a}_\omega^{\dagger \text{cos}} |0\rangle = \int dt \exp(-\gamma|t|) \cos \Omega t \hat{a}_t^\dagger |0\rangle, \quad (28)$$

where the envelope is $h(t)$ and carrier wave is $\cos \Omega t$. Therefore, the conditioned state can be interpreted as a squeezed single-photon state in the cos-sideband wavepacket $\hat{a}^{\text{passive}} = \int dt h(t) \cos \Omega t \hat{a}_t$ and all the other modes are left in the sideband-squeezed state.

Although sideband-cat state can be generated by this method, it can be pointed out that the high frequency sideband is technically challenging to reach for the following reasons; 1. The timing jitter of trigger line electronics mixes sin and cos sideband components. Especially the timing resolution of state-of-the-art APDs, for example 225 ps for SPCM-AQRH-TR series (Excelitas Technologies), will limit the sideband frequency at several hundred MHz. 2. The sideband phase is determined by the detection timing of the trigger photon. 3. The trigger line frequency filter is hard to be realized by simple cavity filters since it should have a strenuous response such that $\pm\Omega$ is selected and $\pm 3\Omega$, $\pm 5\Omega$ and higher order resonances are rejected.

Figure S1B depicts the active subtraction demonstrated in the experiment. The EOM picks up trigger photons from a certain sideband, which fixes the sideband phase of the heralded state irrespective of the photon detection timing. Phase modulation is expressed in the Heisenberg picture as (24)

$$\hat{a}_t^{\text{mod}} = \exp[i\beta \sin(\Omega t + \theta)] \hat{a}_t = \sum_{n=-\infty}^{\infty} J_n(\beta) e^{in(\Omega t + \theta)} \hat{a}_t \quad (29)$$

where J_n is n -th order first kind Bessel function and θ is modulation phase. The frequency-domain expression of Eq.(29) becomes

$$\hat{a}_\omega^{\text{mod}} = J_0(\beta) \hat{a}_\omega + \sum_{n=1}^{\infty} J_n(\beta) \left[e^{in\theta} \hat{a}_{\omega+n\Omega} + e^{-in\theta} \hat{a}_{\omega-n\Omega} \right]. \quad (30)$$

When $\beta \ll 1$, higher order terms can be omitted, giving

$$\hat{a}_\omega^{\text{mod}} \approx \sqrt{1 - \frac{\beta^2}{2}} \hat{a}_\omega + \frac{\beta}{\sqrt{2}} \frac{e^{i\theta} \hat{a}_{\omega+\Omega} + e^{-i\theta} \hat{a}_{\omega-\Omega}}{\sqrt{2}}. \quad (31)$$

This is a sideband-phase-sensitive beamsplitter, whose sideband phase can be tuned by θ . From now on, θ is set at zero. The baseband mode is coupled to the cos-sideband as

$$\hat{a}_{\omega=0}^{\text{mod}} \approx \sqrt{1 - \frac{\beta^2}{2}} \hat{a}_{\omega=0} + \frac{\beta}{\sqrt{2}} \hat{a}_{\Omega}^{\text{cos}}. \quad (32)$$

Cos-sideband modes couple to both baseband and 2Ω modes while the baseband component vanishes in the sin-sideband,

$$\hat{a}_{\Omega}^{\text{cos, mod}} \approx \sqrt{1 - \frac{3\beta^2}{4}} \hat{a}_{\Omega}^{\text{cos}} + \frac{\beta}{\sqrt{2}} \left[\hat{a}_{\omega=0} + \frac{1}{\sqrt{2}} \hat{a}_{2\Omega}^{\text{cos}} \right] \hat{a}_{\Omega}^{\text{sin, mod}} \approx \sqrt{1 - \frac{\beta^2}{4}} \hat{a}_{\Omega}^{\text{sin}} + \frac{\beta}{2} \hat{a}_{2\Omega}^{\text{sin}}. \quad (33)$$

In the time-domain, the assumption $\beta \ll 1$ leads to

$$\hat{a}_t^{\text{mod}} \approx \left[\sqrt{1 - \frac{\beta^2}{2}} + \beta \cos \Omega t \right] \hat{a}_t. \quad (34)$$

Now we consider sideband photon subtraction. The OPO's output mode \hat{a}_t is transformed to \hat{a}_t^{mod} by a phase modulation at the first sideband frequency Ω . The series of a frequency separator and filters are in total an optical low-pass filter represented by a time-domain response function $f(t)$. The filtered mode \hat{a}_t^{trig} is expressed as a sum of transmission response of \hat{a}_t^{mod} and reflection response of \hat{a}_t^{trig} :

$$\hat{a}_t^{\text{trig}} = \int dt' \left[f(t' - t) \hat{a}_{t'}^{\text{mod}} + \left(\delta(t) - f(t' - t) \right) \hat{a}_{t'}^{\text{trig}} \right], \quad (35)$$

where the initial state of \hat{a}_t^{trig} is assumed to be vacuum. Substituting \hat{a}_t^{mod} with Eq. (34), \hat{a}_t^{trig} is split to three terms:

$$\hat{a}_t^{\text{trig}} = \int dt' \left[\sqrt{1 - \frac{\beta^2}{2}} f(t' - t) \hat{a}_{t'} + \beta \cos \Omega t' f(t' - t) \hat{a}_{t'} + \left(\delta(t) - f(t' - t) \right) \hat{a}_{t'}^{\text{trig}} \right]. \quad (36)$$

We assume that the low-pass cutoff is below the first sideband frequency. This derives the following interpretations; the first term is composed of the baseband vacuum component of the OPO's output, and the second term is the downconverted component, which carries photons from the sideband squeezing. A photon detection at $t = \tau$ places ${}_{\text{trig}}\langle 0 | \hat{a}_{\tau}^{\text{trig}}$ on the OPO's output state $|\psi\rangle_{\text{OPO}}$. Here, since the only photon source in \hat{a}_t^{trig} is the second term, the other terms disappear. The conditioned state reads

$$|\psi\rangle_{\tau} = \int dt f(t - \tau) \cos \Omega t \hat{a}_t |\psi\rangle_{\text{OPO}}. \quad (37)$$

Thus, a photon is subtracted from the following sideband-wavepacket mode:

$$\hat{a}_\tau^{\text{sub}} = \int dt f(t - \tau) \cos \Omega t \hat{a}_t. \quad (38)$$

As for conventional baseband photon subtraction schemes, a squeezed single photon state, i.e. an optical SC state is induced by this operation. $\hat{a}_\tau^{\text{sub}}$ and OPO's correlation function determines the SC state's mode $\hat{a}_\tau^{\text{cat}}$ in a similar manner (30) to Eq. (28), giving

$$\hat{a}_\tau^{\text{cat}} = \int dt (f * h)(t - \tau) \cos \Omega t \hat{a}_t, \quad (39)$$

where the envelope function is a convolution of filter response $f(t)$ and OPO's decay function $h(t)$, namely $(f * h)(t) = \int dt' f(t')h(t - t')$. The orthogonal sideband mode

$$\hat{a}_\tau^{\text{SQ}} = \int dt (f * h)(t - \tau) \sin \Omega t \hat{a}_t \quad (40)$$

remains in a squeezed state. Note that τ only appears in the envelope, while the preliminary definition of the sideband phase is given by the downconverting EOM as $\cos \Omega t$. This feature greatly helps us to apply further operations on the generated cat state, since linear operations, for example quantum teleportation or universal squeezing (7), can be applied continuously on the cos-sideband.

Model of sideband homodyne measurement

A time-resolved homodyne measurement gives a way to access multiple DSB modes independently and simultaneously. An ideal homodyne detection is a quadrature measurement of instantaneous mode \hat{a}_t :

$$\hat{X}(t; \phi) = \frac{e^{i\phi} \hat{a}_t^\dagger + e^{-i\phi} \hat{a}_t}{\sqrt{2}}, \quad (41)$$

which contains the information of the quadrature of any longitudinal modes. Quadrature of a wavepacket mode with a real mode function $g(t)$ can be calculated as

$$\hat{X}_g(\phi) = \int dt g(t) \hat{X}(t; \phi). \quad (42)$$

We first multiply the sideband envelope function electrically and continuously by an IQ demodulator. This results in two instantaneous signals

$$\hat{X}^{\text{cos}}(t; \phi) = \cos \Omega t \hat{X}(t; \phi), \hat{X}^{\text{sin}}(t; \phi) = \sin \Omega t \hat{X}(t; \phi). \quad (43)$$

In our experiment, the bandwidth of the homodyne detector around the sideband frequency is not negligible. Thus the detected signal is a convolution with a response function $d(t)$,

$$\hat{X}_d^{\text{cos}}(t; \phi) = \int dt' d(t - t') \cos \Omega(t') \hat{X}(t'; \phi). \quad (44)$$

We assume that the response of the homodyne detector is determined by the first order resonance, which behaves as a single pole low-pass filter around the sideband frequency expressed by

$$d(t) = \exp(-2\pi f_c t)\Theta(t), \quad (45)$$

where f_c is the cut-off frequency, and $\Theta(t)$ is Heaviside step function.

The waveform is digitized with triggers of photon detection events at τ . From now on, we re-label t so that the trigger time τ comes to the origin, thereby shifting the envelope of the wavepacket at the fixed position in the measurement frame. Then the data trace is expressed as

$$\hat{X}_d^{\text{cos}}(t; \phi) = \int dt' d(t-t') \cos \Omega(t'+\tau) \hat{X}(t'+\tau; \phi). \quad (46)$$

The wavepacket of the cat state is identified from the digitized data ensemble by applying independent component analysis (ICA), which detects the non-Gaussianity of the heralded cat mode $\hat{a}_\tau^{\text{cat}}$. We optimized the envelope function $\chi(t)$ of the cat mode minimizing the kurtosis of the quadrature distribution. Thus we expect that the quadrature of the cat state $\hat{X}^{\text{cat}}(\phi)$ is extracted as follows:

$$\hat{X}^{\text{cat}}(\phi) = \int dt \chi(t) \hat{X}_d^{\text{cos}}(t; \phi) = \int dt (f * h)(t) \cos \Omega(t + \tau) \hat{X}(t; \phi). \quad (47)$$

$\chi(t)$ is supposed to be a deconvolution of $d(t)$ from the naive envelope $(f * h)(t)$ in Eq.(39). As long as the detector's response $d(t)$ is narrow enough compared to $(f * h)(t)$, the estimated mode function $\chi(t)$ is non-singular, and the quadrature of the cat state can be numerically extracted. Using the same envelope $\chi(t)$, the orthogonal sideband mode is extracted as

$$\hat{X}^{\text{SQ}}(\phi) = \int dt \chi(t) \hat{X}_d^{\text{sin}}(t; \phi) = \int dt (f * h)(t) \sin \Omega(t + \tau) \hat{X}(t; \phi). \quad (48)$$

Materials and Methods

Experiment

Figure S2 shows the detail of the experiment. The OPO with an FSR of $2\Omega = 1001.2 \text{ MHz}$ includes a type-0 phase matched PPKTP crystal ($1 \text{ mm} \times 1 \text{ mm} \times 10 \text{ mm}$, Raicol), which operates a degenerate parametric down conversion at least over 100 GHz bandwidth. The p-polarized pump light at 430 nm is provided by a second-harmonic-generator cavity driven by an 860 nm continuous-wave seed laser (MBR-110, Coherent). The oscillation threshold of the OPO is measured at 550 mW and the power of the pump light is set at 25 mW, corresponding to the normalized pump amplitude $\varepsilon = 0.21$. The OPO's output coupler mirror with 12% transmissivity corresponds to the line width of $f_{\text{HWHM}} = 10 \text{ MHz}$, or equivalently, the decay constant

$\gamma_{\text{OPO}} = 1/16$ ns. The design parameters of the cavities are summarized in Table S1. The OPO is locked by a 1501.8 MHz detuned locking beam produced by an external cavity diode laser (see Fig. S3) to make it resonant at $\pm\Omega, \pm3\Omega, \dots$ sidebands.

The output squeezed light is modulated by a homemade EOM, which consists of a bulk KTP crystal (1 mm \times 1 mm \times 10 mm, Raicol) and air-core transformer for the resonant matching at 500 MHz. The modulation power is adjusted at 29 dBm so that 2.0% of the light power in 500.6 MHz cos-sideband is downconverted to 0 Hz, corresponding to $\beta^2 = 0.040$ in Eq.(32). As in Eq.(30), part of the optical power is also distributed to the second or higher order harmonic, however, the transfer ratio is below 0.1% and negligible. A high-grade anti-reflection coating suppresses the optical loss below 0.5%. The sideband squeezed light and the downconverted trigger photons are subsequently split by a triangle cavity. The sideband signal light is reflected and measured by a homodyne detection with 0 Hz optical local oscillator (LO). The LO beam is spatially and longitudinally filtered by a mode cleaning cavity. We have developed a resonant homodyne detector for a direct detection of 500 MHz sideband, which is equipped with 98% quantum efficiency Si photodiode (S5971SPL, Hamamatsu Photonics) and has 12.0 dB of shotnoise signal to noise ratio at 500 MHz with 5.0 mW LO (27). The cut-off frequency f_c is measured at 14 MHz by fitting the gain spectrum with Lorentzian function around the resonance peak. Since the electric noise can be equivalently treated as an optical loss (33), we derive a frequency-dependent loss spectrum at below 7% across the OPO's bandwidth. The IQ demodulator (ADL5380, Analog Devices) driven by 500.6 MHz electrical LO downconverts in-phase (cos-sideband) and quadrature (sin-sideband) components of the homodyne detector's signal. They are simultaneously digitized by a 5 Gsamples/s, 12-bit oscilloscope (DSOS204A, Keysight Technologies) with a trigger signal from the APD.

The overall optical efficiency of the setup is estimated as $\eta_{\text{tot}}^{\text{est}} = 0.80$, which includes the OPO's escape efficiency (0.982), the propagation loss (0.035), the interference efficiency with optical LO (0.935), and the detection efficiency of the homodyne measurement (0.91). From Eq.(33), the power transfer ratio at the phase-modulation, $3\beta^2/4 = 0.030$ for cos-sideband and $\beta^2/4 = 0.010$ for sin-sideband, is also to be taken into account.

The trigger photon is further filtered by two Fabry-Perot cavities to reject higher order sideband photons. The response function $\mathcal{T}(t)$ of each filter is exponential decay function characterized by the decay constant γ shown in Table S1:

$$\mathcal{T}(t) = \exp(-\gamma t)\Theta(t). \quad (49)$$

The total response function is a convolution of the three responses. All these filtering cavities are locked by Pound-Drever-Hall method using s-polarized counter-propagating locking beams. The trigger photon is detected by an APD (SPCM-AQRH-16-FC, Excelitas Technologies), supplying a trigger signal which heralds the photon-subtraction event. The total transmission of the

trigger line is 39%, and the total detection efficiency is 10% considering the APD's quantum efficiency of 54% and 50% intrinsic loss at the picking-up modulation.

To control optical phase and sideband phase, a p-polarized reference light is introduced to the OPO through a high-reflection mirror. This light is detuned at 500 kHz and deeply modulated at $\Omega = 500.6$ MHz by a waveguide-type phase modulator (EOSPACE). The relative phase of the downconverting EOM and the electrical LO of the IQ demodulator is adjusted so that they match the modulation phase of the reference light. All these modulation signals are generated from the synchronized direct digital synthesizers (AD9959, Analog Devices). When 0.5 ± 500.6 MHz sideband light goes through the OPO, the parametric amplification generates a difference frequency light at -0.5 ± 500.6 MHz (see Fig. S3). After the EOM, 1 MHz amplitude modulation appears, to which the phase-locked loop (PLL) technique is applied to lock the pumping phase. The optical LO phase is also controlled by PLLs using the 500 kHz signal of the in-phase component of the homodyne detection. The reference beam and cavity-locking beams are chopped during the measurement period and the phase locking are held then. The interval of the sample-and-hold loop is 250 us and the duration of the measurement window is 60 us. To scan the phase of the homodyne measurement, we use an acoust-optic modulator (AOM) to jump the LO phase from the constant locked phase to the arbitrary measurement phase at the beginning of the window.

The event rate of the photon subtraction is 900 counts/s inside the measurement window. Among the triggers, 7 counts/s is fake clicks, which is mainly the dark count of the APD. This replaces 0.8% of the triggered states with non-heralded squeezed states.

Characterization of the sideband squeezed state

Figure S5A shows the squeezing / anti-squeezing spectrum around 500.6 MHz sideband. This data is taken without the APD's trigger signal and the Q component (sin-sideband mode) of the homodyne signal is used. It well matches the theoretical prediction from Eq.(15) with $\epsilon = 0.21$ and $\gamma = 1/(16\text{ns})$ as mentioned above, while we infer the effective efficiency of sin-sideband $\eta^{\text{sin}} = 0.70$ from the fitting. Deducting the 1% power transfer by the phase modulation, we derive the total efficiency η_{tot} at 71% and estimate the effective efficiency of cos-sideband η^{cos} at 68%. We have 9% of excessive loss in η_{tot} over $\eta_{\text{tot}}^{\text{est}}$. We currently do not identify this difference, while we suppose it to be an optical loss of photodiode in the high-frequency region. Thus we assume the actual detection efficiency of the homodyne measurement η_{det} at 83%, as mentioned in the main text.

Figure S5B is the phase scan plot of the squeezing level around 500.6 MHz sideband, where each sample point corresponds to the 36 phases of the homodyne measurement. The phase dependence agrees with the theoretical curve, showing the accuracy of the phase locking and

the phase jump of the LO. The squeezing phase is estimated at 66 degrees by the fitting. Note that the phase of the squeezed state can be easily changed by adjusting the PLL of the pump phase.

Mode estimation and state tomography

8000 traces of the demodulated homodyne signal $X_d^{\cos}(t; \phi)$ and $X_d^{\sin}(t; \phi)$ are collected for equally separated 36 measurement phases. Figure S.6 shows the envelope function of the photon-subtracted mode $\chi(t)$ obtained from the cos-sideband dataset by ICA. The physically measured envelope with the homodyne detector $(\chi * d)(t)$ fits the theoretical envelope function $(f * h)(t)$ that we expected, showing 99% of mode-matching. The quadrature distributions are obtained by multiplying $\chi(t)$ to the datasets. We normalize them with the shotnoise variance of the same wavepacket, which is acquired from the homodyne detection without pumping the OPO.

Recursive maximum-likelihood estimation (29) is used to reconstruct the density matrix in Fock basis with a photon-number cutoff of 13. Figure S7 shows the density matrices estimated from the quadrature distributions of cos- and sin- sideband. Wigner function representation in the main text is obtained from the density matrix. To estimate the statistical error of the Wigner function, we use bootstrap method (34), where the variance of the Wigner function is calculated from 100 times of trial virtually performed by resampling 8000 quadratures from the raw data for each phase.

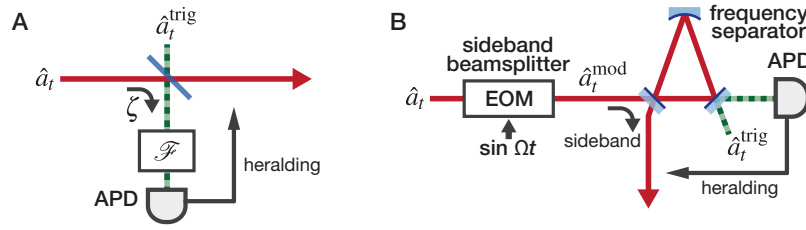


Fig. S1. Schematics of photon subtraction from double-sideband. **(A)** Passive subtraction. A beamsplitter with the reflectance ζ picks up trigger photons. Sideband photons are selected by a frequency filter \mathcal{F} and detected by an avalanche photodiode (APD). **(B)** Active subtraction using a phase modulation. Trigger photons are downconverted to the baseband by an electro-optic modulator (EOM) and spatially separated by an optical cavity.

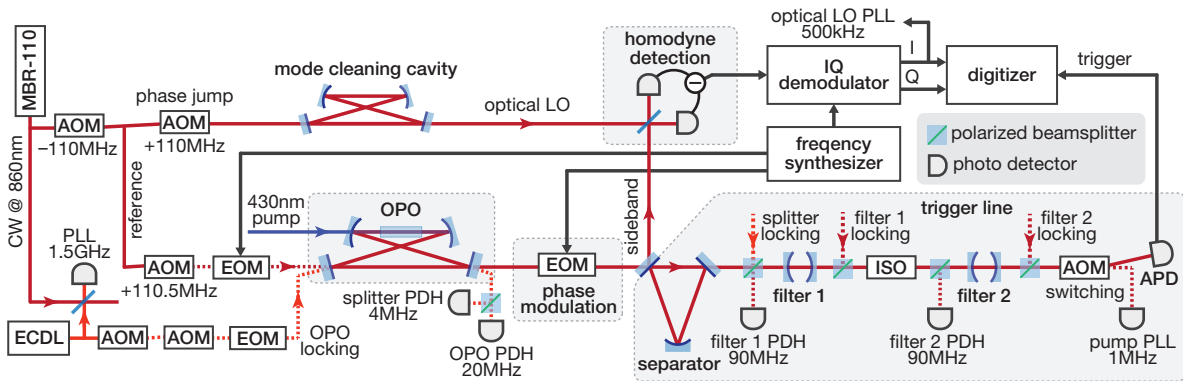


Fig. S2. Experimental setup. Solid lines are continuous wave laser and dashed lines indicates chopped light. OPO: optical parametric oscillator; CW: continuous-wave; APD: avalanche photodiode; EOM: electro-optic modulator; LO: local oscillator; AOM: acoust-optic modulator; ECDL: extra cavity diode laser; ISO: optical isolator; PDH: Pound-Drever-Hall locking, PLL: phase-locked loop. I and Q denote in-phase and quadrature signals.

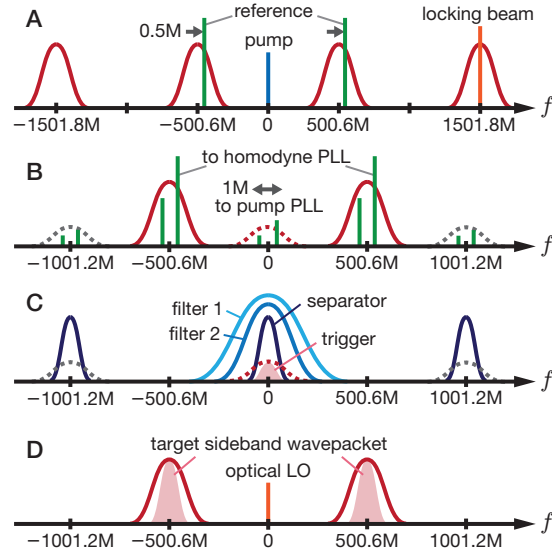


Fig. S3. Frequency diagram of the experiment. Frequency f is expressed in Hz. **(A)** OPO's resonance, and pump / locking / reference beam. **(B)** Spectrum of the squeezed light and the reference beam after going through the OPO and downconverting EOM. **(C)** Filtering spectrum of the trigger line. The resonance of the separator cavity and two filtering cavity is indicated. **(D)** The frequency structure of the homodyne detection.

	f_{FSR}	f_{HWHM}	γ
OPO	1.0012 GHz	10 MHz	1/16 ns
separator	1.00 GHz	5.3 MHz	1/30 ns
filter 1	75 GHz	72 MHz	1/2.2 ns
filter 2	52 GHz	50 MHz	1/3.2 ns

Table S1. Parameters of the OPO and the trigger line filters. f_{FSR} : free spectral range, f_{HWHM} : linewidth in half-width at half-maximum (HWHM), γ : decay constant.

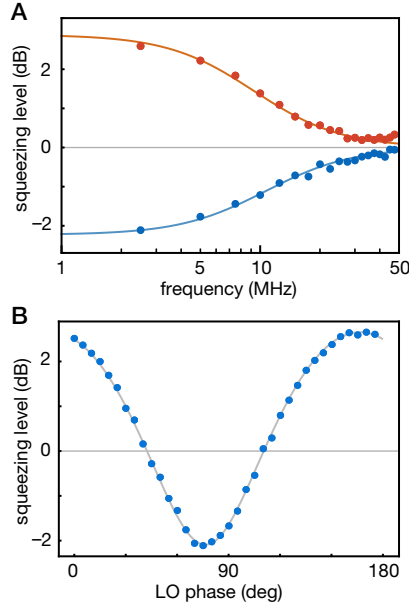


Fig. S5. Characterization of the sideband squeezed state. **(A)** Squeezing / anti-squeezing spectrum around the 500.6 MHz sideband. The power prospectus is calculated by fast Fourier transformation of the demodulated Q signal of homodyne detection. This is an average of 8000 traces of 400 ns period, and normalized by the shotnoise power. Theoretical curves are also shown. **(b)** Phase scan plot of the quadrature variance, obtained from the power spectrum by averaging the DC-5 MHz component power.

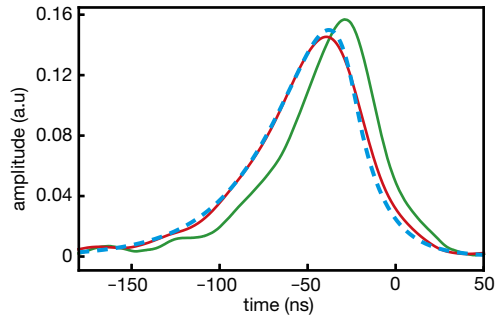


Fig. S6. Envelope functions of the sideband cat state. Green curve: analytical envelope function $\chi(t)$ estimated by ICA; red curve: physically measured temporal mode envelope $\xi(t)$, calculated as $(\chi * d)(t)$. This is shown in the main text; blue-dashed curve: theoretical prediction of the envelope function of the cat state $(f * h)(t)$. All these wavepackets are normalized by 2-norm.

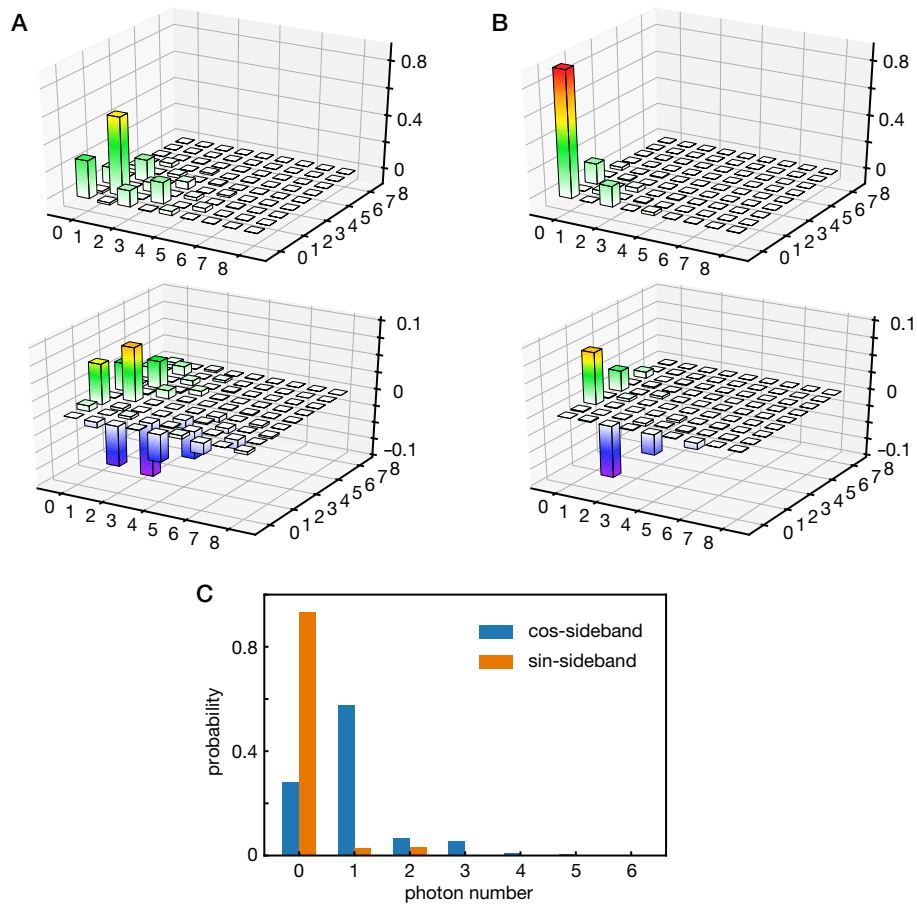


Fig. S7. Density matrices of (A) cos-sideband mode and (B) sin-sideband mode. The real part (above) and imaginary part (below) is separately plotted. Only the subspace up to 8 photons is shown. (C) photon number distributions.